Scilight

Modern Nuclear and Radiochemistry
https://www.sciltp.com/journals/mnr



Article

Radiation-Resistant Betaine Hydrochloride for Facile Ln/An Group Separation via Selective Dissolution

Zhuo-Fan Jin [1,2], He-Xiang Jia [1,2], Bing-Qing Wei [1,2], Qing-Gang Huang [1], De-Sheng Chen [1], Xiao-Jie Yin [1], Shi-Wei Cao [1], Zhi Qin [1] and Fang-Li Fan [1,*]

[1] Institute of Modern Physics, Chinese Academy of Sciences, Lanzhou 730000, China
[2] School of Nuclear Science and Technology, University of Chinese Academy of Sciences, Beijing 100000, China
* Correspondence: fanfangli@impcas.ac.cn

How To Cite: Jin, Z.-F.; Jia, H.-X.; Wei, B.-Q.; et al. Radiation-Resistant Betaine Hydrochloride for Facile Ln/An Group Separation via Selective Dissolution. *Modern Nuclear and Radiochemistry* **2026**, *1*(1), 4.

Received: 6 July 2026
Revised: 6 September 2026
Accepted: 23 October 2026
Published: 2 November 2026

Abstract: The separation of lanthanide (Ln) fission products from actinide (An) matrices is essential for reducing neutron poisons and improving spent nuclear fuel reprocessing. Herein, aqueous betaine hydrochloride (HbetCl) is developed as a radiation-resistant, single-component medium for facile Ln/An group separation through selective dissolution. Under mild conditions, HbetCl efficiently dissolves lanthanide sesquioxides (Ln_2O_3) from simulated spent nuclear fuel, achieving over 95% Ln removal, while actinide dioxides remain largely undissolved and can be directly recovered as solid residues by simple centrifugation. The separation performance is well preserved after γ-irradiation up to 1000 kGy, as demonstrated by the nearly 97% leaching of neodymium (Nd). In contrast, AnO_2 exhibits strong resistance toward HbetCl dissolution. In particular, experiments using radioactive $^{243}AmO_2$ further confirm that the selective-dissolution strategy is applicable not only to UO_2-based matrices but also to representative minor actinide oxides, highlighting its relevance to practical spent-fuel reprocessing. Density functional theory (DFT) calculations indicate that betaine (BET) facilitates Ln_2O_3 dissolution by stabilizing dissolved lanthanide species through hydrogen-bonding interactions, thereby providing molecular-level insight into the selectivity of the process. Overall, the radiation-resistant HbetCl enables a mild, simple, and efficient route for Ln/An group separation by preferentially transferring lanthanides into solution while retaining actinides in the solid phase. This strategy reduces actinide carryover into the liquid phase and provides a promising platform for advanced spent nuclear fuel reprocessing toward a closed nuclear fuel cycle.

Keywords: lanthanides; actinides; selective dissolution; separation; spent nuclear fuel

1. Introduction

In spent nuclear fuel reprocessing, the separation of lanthanide fission products from actinide oxide matrices is closely related to neutron economy, radioactive waste management, and the development of closed nuclear fuel cycles. Selective dissolution of metal oxides has emerged as an attractive strategy for such separations because it enables direct solid–liquid partitioning by exploiting differences in lattice stability, surface reactivity, acid-base behavior, and metal-ligand coordination [1–3]. Compared with conventional approaches involving high-temperature treatment, concentrated mineral acids, or multistep solvent extraction, selective dissolution offers the possibility of reducing energy input, reagent consumption, and secondary waste generation [4,5]. For nuclear-relevant applications, however, the dissolution medium must satisfy additional requirements, including chemical selectivity under irradiation, limited actinide carryover into liquid streams, and compatibility with simplified radioactive-waste management. Therefore, the rational design of simple, inexpensive, water-compatible, and



Copyright: © 2026 by the authors. This is an open access article under the terms and conditions of the Creative Commons Attribution (CC BY) license (https://creativecommons.org/licenses/by/4.0/).
Publisher's Note: Scilight stays neutral with regard to jurisdictional claims in published maps and institutional affiliations.

radiation-tolerant dissolution media that can selectively dissolve targeted oxide phases while leaving chemically similar oxides undissolved remains a significant challenge.

This challenge is especially pronounced for f-element oxides. Lanthanides and actinides possess similar ionic radii, preferred oxidation states, and coordination environments, making their separation one of the most difficult problems in inorganic and separation chemistry [6–8]. Although the underlying chemistry is also relevant to rare-earth recovery and complex oxide recycling, it becomes particularly demanding in nuclear fuel-cycle scenarios because separation must be achieved in chemically complex and highly radioactive environments. The difficulty is not limited to nuclear fuel reprocessing; it is also relevant to rare-earth recovery, critical-metal recycling, and the purification of complex oxide mixtures. Among various separation strategies, selective dissolution provides a conceptually simple route because it avoids complete dissolution of all components followed by downstream separation. Instead, it seeks to selectively convert only the target oxide phase into soluble metal species, while the non-target oxide remains in the solid residue. Such a strategy is particularly attractive when the coexisting oxides differ in lattice energy, oxidation state stability, defect chemistry, or susceptibility to proton- and ligand-assisted dissolution [3,9,10]. In the context of spent nuclear fuel treatment, the selective dissolution of lanthanide oxides from actinide-containing oxide matrices represents a promising example of this broader chemical principle. During reactor operation, uranium oxide fuel undergoes fission and neutron-capture reactions, producing fission products (including lanthanides) and trans-uranic actinides. Because several lanthanide fission products, particularly Sm, Eu, and Gd, have large neutron-absorption cross sections, their accumulation can adversely affect neutron economy. Their preferential removal is therefore desirable, whereas uranium, plutonium, and minor actinides such as neptunium and americium may be retained or recovered for subsequent management, transmutation, or fuel refabrication [11–14]. Conventional spent fuel reprocessing, such as the PUREX process, has demonstrated effective recovery of uranium and plutonium; however, the efficient separation and management of minor actinides remain challenging. This limitation has motivated the development of alternative fuel-cycle concepts, including the Accelerator-Driven Advanced Nuclear Energy System (ADANES) proposed by Chinese Academy of Sciences [15]. ADANES couples an accelerator-driven subcritical system with an advanced fuel-cycle strategy for the transmutation and utilization of minor actinides. Its external high-flux neutron source enables flexible fuel transmutation and renders the system tolerant to complex spent fuel compositions, relaxing the stringent removal requirements for most fission products in conventional reprocessing. Nevertheless, lanthanide fission products must be separated, if retained within the fuel matrix, they possess large neutron absorption cross sections that degrade neutron economy. In the ADANES cycle, spent fuel first undergoes preliminary high-temperature dry treatment to eliminate volatile fission products. On this basis, selective lanthanide dissolution is implemented as a core preliminary fuel-cleaning and group-separation operation to remove neutron-absorbing impurities. The partially purified fuel matrix, with neutron-poisoning lanthanides removed, can be directly reused in subcritical reactors, avoiding cumbersome full chemical separation and facilitating industrial deployment. It should be noted that uranium and transuranic actinides including minor actinides are retained in the actinide-bearing solid residue for subsequent conditioning and fuel refabrication. Accordingly, the value of selective lanthanide dissolution lies not in replacing mature aqueous reprocessing technologies, but in removing harmful neutron poisons while limiting the actinide fractions transferred into the aqueous phase, which optimizes the efficiency of the pretreatment and group-separation process. Conventional aqueous reprocessing relies heavily on strong acids and solvent extraction, and although these processes are technologically mature, they can involve complicated flowsheets, large volumes of liquid waste, and organic extractants [16,17]. In this context, the HbetCl-based strategy investigated here is intended to preferentially remove lanthanide neutron poisons while retaining the actinide-containing solid matrix. At its present stage of development, it should be regarded as proof-of-concept research and a potential technical reserve, rather than as a mature standalone process capable of producing fuel-grade actinide products directly from actual spent nuclear fuel. Practical implementation would require integration with upstream removal of volatile and semi-volatile fission products and downstream purification, solvent regeneration, residue conditioning, and fuel refabrication operations.

Previous studies have demonstrated the feasibility of selective oxide dissolution using task-specific ionic liquids, ligand-assisted ionic-liquid media, and salt-based systems. For example, Dupont and Binnemans reported that the carboxyl-functionalized ionic liquid protonated betaine bis(trifluoromethylsulfonyl)imide, [Hbet][Tf_2N], can selectively dissolve the rare-earth-containing red phosphor Y_2O_3:Eu^{3+} from lamp phosphor waste while leaving other phosphors, glass particles, and alumina largely undissolved [18]. More directly relevant to lanthanide–actinide oxide separation, Verma and co-workers showed that Eu_2O_3 can be rapidly and selectively dissolved in a ligand-assisted room-temperature ionic-liquid medium containing 2-thenoyltrifluoroacetone, whereas UO_2 and AmO_2 exhibit very poor dissolution [11]. In parallel, salt-based strategies have also been explored; for instance, NH_4Cl-assisted dissolution in LiCl-KCl molten salt was shown to convert Ln_2O_3 into soluble chlorides while UO_2

remained predominantly in the solid phase [19]. Other systems, including deep eutectic solvents, H_2SO_4, MSA, and HCl/NaCl, have also been investigated for selective rare-earth or lanthanide dissolution [2,20,21]. These studies collectively indicate that oxide dissolution can be controlled through a combination of medium acidity, ligand coordination, chloride participation, hydration environment, and oxide lattice stability. However, many reported systems still suffer from limitations such as high viscosity, high cost, hydrophobicity, uncertain radiolytic stability, use of organic components, or the need for additional reagents.

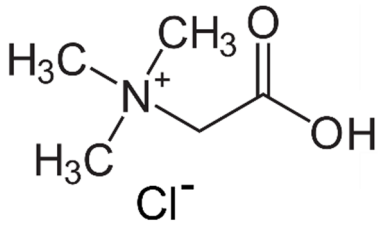
Betaine hydrochloride (HbetCl) represents a simple and sustainable platform for selective oxide dissolution. This inexpensive, commercially available, and highly water-soluble betaine-derived salt avoids hydrophobic fluorinated anions and bulky organic extractants, yet combines acidity, oxygen-donor coordination ability, hydrogen-bonding capacity, and chloride participation within a single small-molecule medium [22,23]. The protonated carboxyl group may promote acid-assisted cleavage of metal-oxygen bonds, while deprotonated betaine can stabilize dissolved metal ions through carboxylate coordination. In parallel, chloride may further modulate metal speciation through ion pairing or secondary coordination [24,25]. Compared with hydrophobic betainium ionic liquids such as [Hbet][Tf_2N], HbetCl offers clear advantages in cost, accessibility, water compatibility, and operational simplicity [26,27]. More importantly for spent-fuel-related separations, its single-component aqueous nature may simplify process design, reduce reliance on conventional organic extractants, and facilitate direct solid–liquid separation between dissolved lanthanides and retained actinide dioxide phases. Nevertheless, its direct use as a sole aqueous dissolution medium for selectively dissolving lanthanide oxides while retaining actinide dioxides, especially under ionizing-radiation conditions relevant to nuclear fuel reprocessing, has remained largely unexplored.

In this study, we employed HbetCl as a simple aqueous medium to achieve the selective dissolution of lanthanide oxides from simulated spent fuel and the concomitant group recovery of actinide dioxides. Using HbetCl alone, without any auxiliary reagents, lanthanide oxides were efficiently converted into soluble species, while the UO_2 matrix remained largely undissolved and could be recovered as a solid residue. Density functional theory (DFT) calculations further supported the proposed dissolution mechanism, showing that betaine can stabilize lanthanide complexes through hydrogen-bonding interactions, thereby facilitating the dissolution process. In addition to its strong solubilizing ability, HbetCl exhibited exceptional radiolytic stability, further highlighting its potential applicability under spent nuclear fuel reprocessing conditions. Overall, this work provides a simple, environmentally friendly, and efficient strategy for separating lanthanide fission products from actinide oxide matrices, and may contribute to the development of more sustainable spent fuel reprocessing technologies.

2. Experimental Section

2.1. Materials and Equipment

All chemicals were commercially available and used as received, without further purification. UO_2 was purchased from China North Nuclear Fuel Co., Ltd. (Baotou, China). ThO_2 was obtained by decomposing from $Th(NO_3)_4$ at 900 °C for 4 h. Betaine hydrochloride (HbetCl) (99%) and all lanthanide oxides were purchased from Alfa Aesar (Tianjin China) with AR degree. The structural formula of HbetCl is shown in Scheme 1.



Scheme 1. Chemical structure of betaine hydrochloride (HbetCl).

Water was always of ultrapure quality, deionized to a resistivity of >18.2 MΩ cm with a Milli-Q® Academic ultrapure water system.

Inductively coupled plasma optical emission spectrometer (ICP-OES; Agilent, type 5100SVDV, Agilent Technologies, Santa Clara, CA, USA) were used to monitor the metal extent of separation process. X-ray Powder Diffraction (XRD) patterns were obtained using a PANalytical X'Pert^3 Powder diffractometer (Malvern Panalytical, Almelo, The Netherlands). The ESI-MS spectra were recorded on a Bruker micro TOF Q II spectrometer (Bruker Daltonics, Bremen, Germany). Thermo Evolution 300 UV-Vis spectrophotometer (Thermo Fisher Scientific, Madison, WI, USA) and Bruker Tensor 27 FTIR spectrometer (Bruker Optik GmbH, Ettlingen,

Germany) were used for measurement of UV-Vis absorption spectra and FTIR spectra, respectively. The sample of radioactivity $^{243}AmO_2$ was measured by an HPGe γ-ray detector (EG&G Ortec GEM50P4-83 (ORTEC, Oak Ridge, TN, USA) with a relative efficiency of 50%) at 30 cm distance and analyzed by gamma ray spectrometry system (DSPEC 50/50A, ORTEC, Oak Ridge, TN, USA) with GammaVision® software (ORTEC, Oak Ridge, TN, USA).

2.2. Preparation of Simulated Spent Nuclear Fuel

The simulated spent nuclear fuel (SIMFUEL) was prepared by thoroughly mixing predetermined amounts of UO_2 with Nd_2O_3 powder. Subsequently, in order to ensure uranium form as UO_2, the mixture was treated at fixed temperature through 4% H_2-Ar for 4 h using a high-temperature furnace. No pellet pressing or compaction was performed prior to heat treatment. The baseline SIMFUEL sample contained approximately 4.98 wt% Nd. A series of samples heat-treated at reduction temperatures ranging from 1000 to 1500 °C were prepared to examine the separation performance. Although selected powder samples were heat-treated at temperatures as high as 1500 °C to investigate the influence of thermal-treatment temperature, this procedure did not constitute conventional ceramic-fuel fabrication. Moreover, to examine the influences of Nd amount on the dissolution, the different simulated spent nuclear fuel samples with a wide Nd content range (0.61~15%) were prepared. A multi-lanthanide SIMFUEL sample was also prepared to evaluate the simultaneous dissolution and separation of different lanthanide fission products. Calculated amounts of Nd_2O_3, Sm_2O_3, Eu_2O_3, and Gd_2O_3 powders were mixed homogeneously with UO_2 powder. The resulting mixture was heat-treated at 1000 °C under flowing 4 vol% H_2–Ar for 4 h using the same procedure described above. The elemental contents of Nd, Sm, Eu, and Gd in this sample were 5.34, 5.80, 6.28, and 6.33 wt%, respectively. This sample was also tested as a heat-treated powder mixture rather than as a densified ceramic pellet.

The SIMFUEL materials used in this study should therefore be regarded as composition-controlled chemical surrogates, rather than complete microstructural replicas of real spent nuclear fuel. Actual spent fuel consists of a dense, irradiated ceramic matrix containing irradiation-induced lattice defects, grain boundaries, pores, fission-gas bubbles, compositional gradients, and multiple secondary phases. In real fuel, lanthanide fission products can exist as lattice-substituted species, grain-boundary segregates or components of complex oxide phases. In contrast, the present SIMFUEL was fabricated from well-defined oxide powders and contains no irradiation-induced defects. In addition, the greater accessible surface area of the powder samples may result in faster dissolution kinetics than those of dense spent-fuel pellets. Consequently, the present SIMFUEL system was designed to provide a controlled platform to evaluate the fundamental chemical selectivity of the HbetCl-based dissolution process.

2.3. Dissolution and Separation Experiments

The dissolution experiments were performed according to the procedure previously reported [28]. The following conditions were kept consistent for all experiments except where otherwise noted: (i) a volume of 2 mL betaine hydrochloride aqueous solution (1M) was used; (ii) 100 mg of simulated spent nuclear fuel with a reduction temperature of 1000 °C was maintain a constant solid-to-liquid ratio (50 $g \cdot L^{-1}$); (iii) all experiments were carried out on a heating plate with an integrated magnetic stirrer; (iv) dissolution experiments were performed at 40 °C for 1 h; (v) after dissolution, all separation was assisted by centrifugation for 5 min at 7000 rpm; and (vi) experiments were done in triplicate. Finally, the concentration of metal in the betaine hydrochloride solution was analyzed by ICP-OES. The dissolution efficiency (E) of Nd_2O_3 (or UO_2) and separation factor (SF) were determined by the following formulas [29].

$$E = \frac{C_m \times V}{m} \times 100\%$$

$$SF = \frac{E_{Nd}/(100 - E_{Nd})}{E_U/(100 - E_U)}$$

The C_m denotes the mass concentration of metal in betaine hydrochloride solution. The V means the volume of betaine hydrochloride solution and the m is the original mass of metal before dissolution. The E_{Nd} and E_U represent the dissolution efficiency of metal *Nd* and *U*, respectively.

2.4. Computational Details and Theoretical Models

All calculations were carried out with the spin-unrestricted density functional theory (DFT) utilizing the DMol^3 module of the Materials Studio software. The exchange-correlation interactions were treated using the generalized gradient approximation (GGA) with the Perdew-Burke-Ernzerhof (PBE) functional and Grimme's DFT-D3 correction were employed to account for weak interactions such as long-rage van der Waals

intermolecular and dispersive intermolecular interactions. For the computational settings, the DND 4.4 basis set was used. The convergence criterion was set to 10^{-6} au in self-consistent field computation, and the real space cutoff radius of atomic orbital was set as 4.9 Å. The geometry optimization was carried out until the convergence threshold of 1×10^{-5} Ha for energy, 2×10^{-3} Ha/Å for force, and 5×10^{-3} Å for displacement [30,31].

2.5. Irradiation Experiments

Irradiation of sample was performed at ambient temperature in Tianchen Irradiation Technology Co. Ltd. (Lanzhou, China). The Cobalt 60 Gamma Facility was used as the gamma source with 1.93 kGy·h^{-1} dose rate. Some betaine hydrochloride solid samples were also irradiated using a ^{60}Co γ-ray source at the Department of Applied Chemistry of Peking University, with an average dose rate of approximately 210 Gy·min^{-1}. The dose rate was monitored using a Fricke dosimeter placed at the sample position. The samples were stored in polypropylene tubes, closed with a plastic lid and sealed with Paraflm® in order to avoid any sample leakage during irradiation. The HbetCl samples were characterized for their structural changes before and after irradiation by FTIR, UV and ESI-MS analysis.

3. Results and Discussion

3.1. Selective Dissolution of Nd_2O_3 from Simulated Spent Nuclear Fuel

In this study, we developed a simple aqueous HbetCl-based selective dissolution process for separating lanthanides from actinide-containing matrices in simulated spent nuclear fuel. The overall concept of the HbetCl-mediated selective dissolution strategy is illustrated in Figure 1. In this process, lanthanide oxides in simulated spent nuclear fuel are preferentially dissolved into the aqueous HbetCl phase under mild conditions, whereas actinide dioxides remain predominantly in the solid phase. This distinct dissolution behavior enables the separation of lanthanides from actinide-containing oxide matrices through a simple solid-liquid separation step. Based on this concept, the selective dissolution performance, lanthanide recovery, actinide retention, radiation stability, and dissolution mechanism of the HbetCl system were systematically investigated.

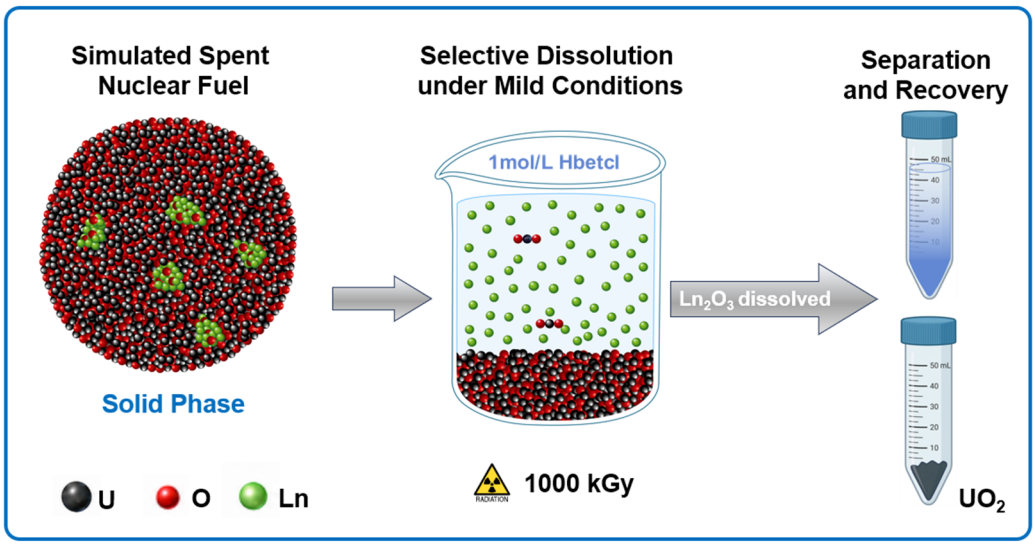


Figure 1. Selective dissolution strategy for lanthanide removal and actinide dioxide recovery from simulated spent nuclear fuel using aqueous HbetCl.

To first verify the intrinsic dissolution behavior of different oxides in HbetCl, individual Nd_2O_3, UO_2, and U_3O_8 powders were examined as model substrates (Figure S2). The HbetCl solution achieved complete dissolution of Nd_2O_3, while only a tiny fraction of uranium oxides dissolved under identical conditions. This drastic difference in dissolution efficiency between Nd_2O_3 and uranium oxides demonstrates the great potential of HbetCl for separating lanthanides from actinides in spent nuclear fuel. After that, a simulated spent nuclear fuel containing Nd_2O_3 and uranium oxides was further employed to evaluate whether such selectivity could be retained in a mixed oxide system. As shown in Figure 2, HbetCl preserved its preferential dissolution behavior toward Nd_2O_3 in the

simulated spent nuclear fuel. Nearly quantitative dissolution of Nd was achieved, with more than 95% of Nd entering the liquid phase, whereas only 1% of uranium was dissolved under the same conditions. Notably, although the dissolution ratio of uranium is extremely low, the absolute mass of dissolved U cannot be neglected due to its dominant proportion in the original SIMFUEL. Even so, the remarkable discrepancy in leaching efficiency firmly verifies the excellent selectivity of HbetCl for Nd_2O_3 over uranium oxides.

After establishing the feasibility of selective Nd_2O_3 dissolution from the simulated spent nuclear fuel, the effect of HbetCl concentration on the dissolution behavior and separation performance was first investigated to identify a suitable dissolution medium. The separation factor between Nd and U increased slightly with increasing HbetCl concentration; however, the dissolution efficiencies of both Nd_2O_3 and uranium oxides showed no significant concentration dependence within the investigated range. Therefore, 1 M aqueous HbetCl was selected as the preferred dissolution medium for subsequent separation studies, considering both dissolution performance and reagent economy. The much higher dissolution efficiency of Nd_2O_3 compared with uranium oxides can be attributed to the relatively facile release of Nd^{3+} from the Nd_2O_3 lattice [32]. In contrast, the uranium oxide matrix remained predominantly in the solid phase, allowing the actinide-containing residue to be readily recovered by simple centrifugation. This result agrees well with our previous study on the [Hbet][Tf_2N] system [28], in which the carboxylate functionality of the $[Hbet]^+$ cation was identified as the key structural moiety responsible for selective oxide dissolution. Taken together, these results demonstrate that HbetCl provides an efficient and highly selective dissolution strategy for separating lanthanide oxides from uranium oxide matrices in simulated spent nuclear fuel.

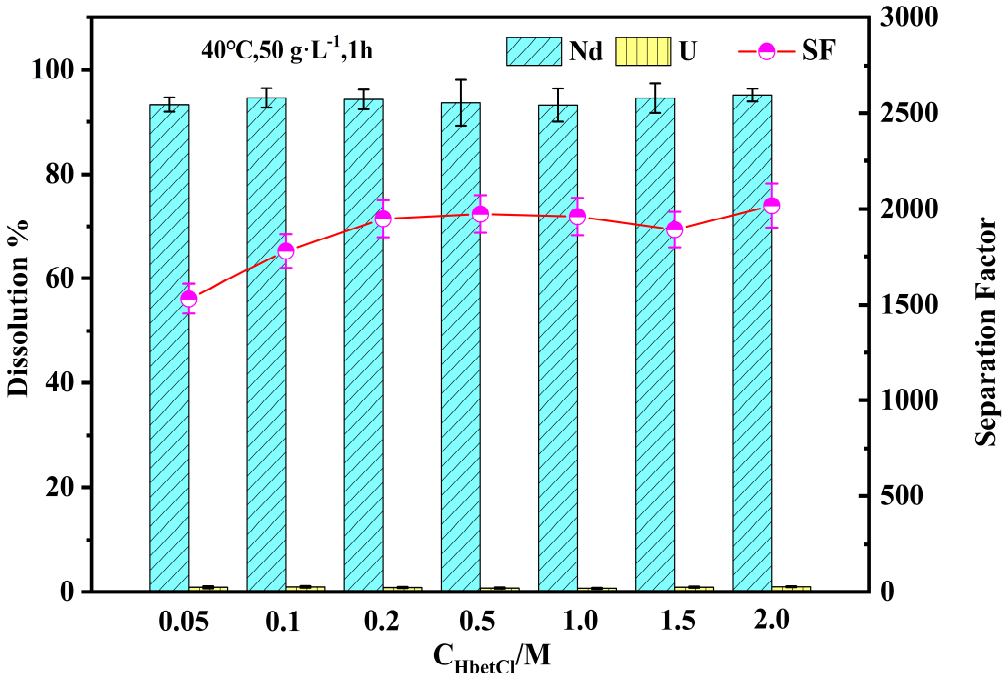


Figure 2. Effect of HbetCl concentration on the selective dissolution of Nd_2O_3 from simulated nuclear fuel.

HbetCl retained highly selective Nd dissolution over a broad range of Nd loadings in the simulated spent nuclear fuel, demonstrating its robustness toward variations in lanthanide content as illustrated in Figure 3. This evaluation is important because the inventory of lanthanide fission products in spent nuclear fuel varies with irradiation history and generally increases with fuel burnup. In particular, Nd is a representative stable lanthanide fission product and is widely used as a burnup indicator [33]. Therefore, examining the effect of initial Nd concentration provides a practical assessment of whether the HbetCl system can maintain its separation performance under different lanthanide inventories. Accordingly, simulated spent nuclear fuel samples with varying Nd contents were treated with HbetCl under the optimized conditions established above. HbetCl consistently exhibited much higher dissolution activity toward Nd than toward U under all tested conditions. Even when the initial Nd content was increased to 15%, the dissolution efficiency of Nd remained as high as 97%. In contrast, uranium dissolution was nearly independent of the Nd content and remained at approximately 1%, confirming the excellent selectivity of HbetCl for Nd over U. Among the tested samples, the lowest loading corresponds to 0.61 wt% total lanthanides, which better approximates realistic spent-fuel conditions. This low-lanthanide sample exhibited selective-dissolution behavior comparable to that observed for the 5 wt% Nd-bearing

sample. Therefore, the 5 wt% Nd formulation was adopted for our main experiments, as it yields sufficiently high Nd concentrations to enable reliable quantitative analysis and effectively reduces relative uncertainties in compositional and solid-phase characterization. Notably, the UO_2 matrix was retained predominantly in the solid phase after dissolution and could be readily recovered by simple solid–liquid separation. These results further confirm the practical feasibility of HbetCl as a simple, additive-free medium for selectively separating lanthanide oxides while simultaneously enabling the recovery of solid UO_2 from simulated spent nuclear fuel. Such performance can be attributed to the combination of high Nd dissolution efficiency, negligible uranium co-dissolution, operational simplicity, and the ready availability of HbetCl.

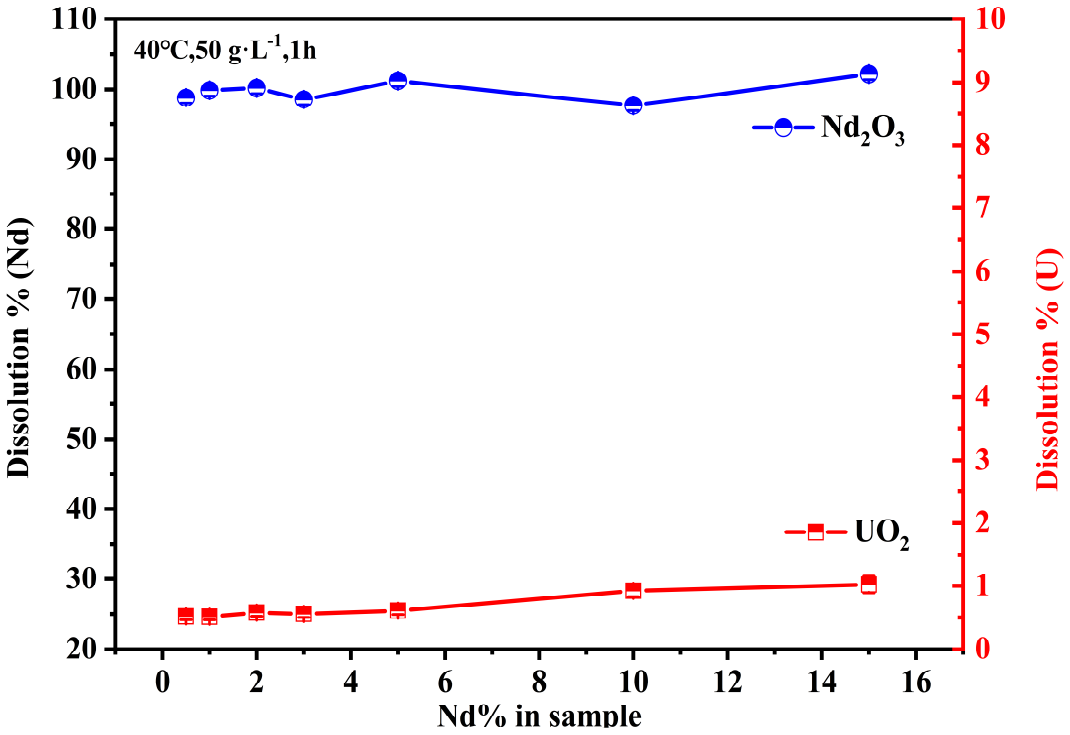


Figure 3. Dissolution of Nd_2O_3 and UO_2 from simulated nuclear fuel.

Even for thermally treated SIMFUEL-type samples designed to more closely mimic spent nuclear fuel, HbetCl retained the ability to selectively remove Nd while preserving most of the UO_2 matrix as a recoverable solid (Figure 4). This pretreatment is important because fission-product lanthanides in irradiated oxide fuels are not simply present as physically mixed oxides, but are commonly incorporated into, dissolved in, or strongly associated with the UO_2-based fuel matrix. Therefore, thermally treated SIMFUEL-type materials are widely used to better reproduce the chemical state and microstructural features of spent nuclear fuel [34–36]. To further evaluate the practical applicability of HbetCl under more realistic fuel-matrix conditions, simulated spent nuclear fuel samples were subjected to reductive thermal treatment at elevated temperatures, and their selective dissolution behavior was then investigated in 1 M HbetCl solution. Under mild dissolution conditions, the accessibility of Nd_2O_3 decreased markedly with increasing pretreatment temperature, whereas uranium dissolution remained very limited. As shown in Figure S4, after dissolution at 40 °C for 2 h, the Nd dissolution efficiency decreased from 45% to 13% when the pretreatment temperature was increased from 1300 °C to 1500 °C. This decrease may be attributed to the enhanced densification of the oxide matrix, reduced accessibility of Nd-containing phases, and the formation of more stable Nd-U-O species during high-temperature treatment. To overcome this reduced dissolution efficiency, the dissolution temperature and stirring time were subsequently increased. As expected, a pronounced improvement in Nd removal was observed at 80 °C. For the sample pretreated at 1300 °C, the Nd dissolution efficiency increased from 57.87% to 82.22% when the dissolution time was extended to 24 h. Similarly, the Nd dissolution efficiencies of the samples pretreated at 1400 °C and 1500 °C were significantly improved to 71.77% and 62.80%, respectively. These results indicate that higher dissolution temperature and prolonged stirring are favorable for promoting Nd removal from the thermally treated oxide matrix. It should be noted that the enhanced Nd dissolution was accompanied by a moderate increase in uranium co-dissolution compared with the experiments conducted at 40 °C. After dissolution at 80 °C for 24 h, the uranium dissolution efficiencies were 13.19%, 12.69%, and 6.56% for the samples pretreated at 1300, 1400, and 1500 °C, respectively. Nevertheless,

considering that UO_2 is the dominant species in spent nuclear fuel, the majority of the uranium oxide matrix remained in the solid phase after treatment. In particular, approximately 90% of UO_2 could still be recovered as a solid residue, indicating that the HbetCl-based dissolution strategy maintains a meaningful degree of selectivity even for highly treated SIMFUEL-type materials. Although enhanced Nd removal under intensified dissolution conditions was accompanied by a certain increase in uranium co-dissolution, these results demonstrate the potential of HbetCl for separating lanthanide oxides from UO_2-based matrices and provide a promising basis for future application to real spent nuclear fuel systems.

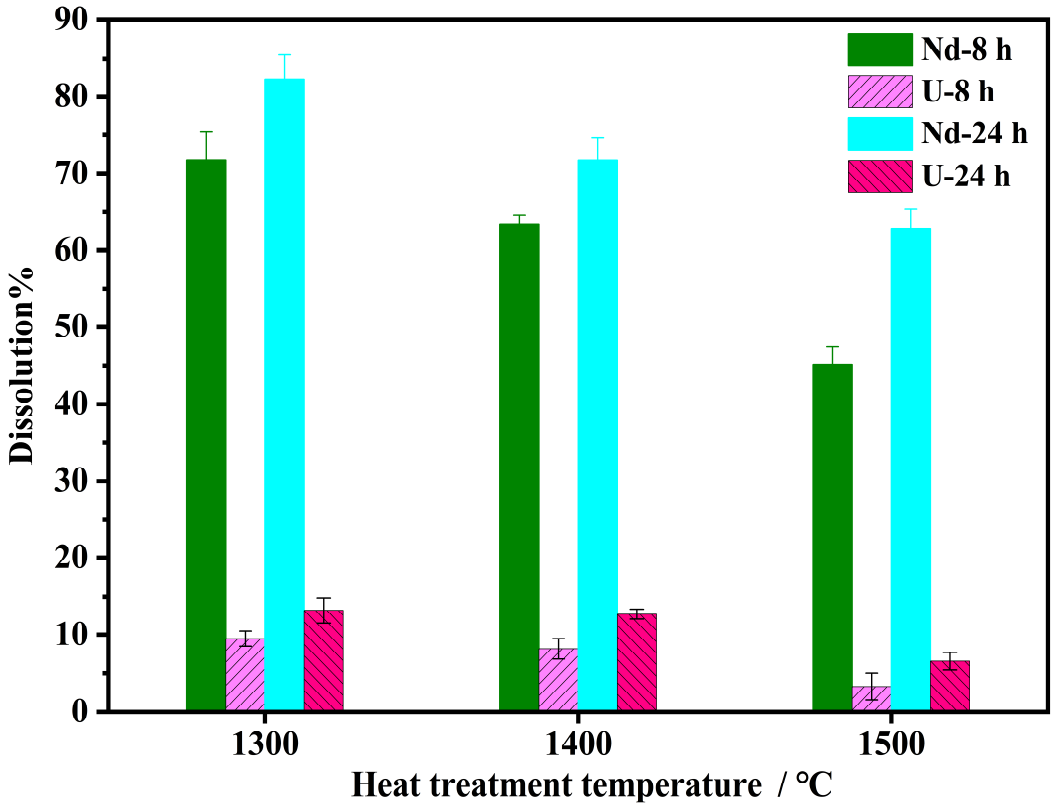


Figure 4. Dissolution separation of Nd_2O_3 from simulated nuclear fuel at 80 °C.

After selective dissolution, the solid residue was characterized by SEM-EDS to evaluate the removal of Nd from the simulated spent nuclear fuel. As shown in Figure 5, the pristine sample exhibited an obvious Nd distribution, represented by green signals in the EDS elemental mapping, together with a uniformly distributed U signal in the UO_2 matrix. After treatment with HbetCl, the Nd signals in the residual solid almost disappeared, whereas the U signals remained broadly distributed throughout the solid residue. This result indicates that Nd was nearly completely removed from the simulated spent nuclear fuel, while the UO_2 matrix was largely retained in the solid phase. To quantitatively confirm the separation efficiency, the recovered UO_2 residue was further analyzed by ICP-OES. The residual Nd content in the recovered UO_2 product was only 0.13%, corresponding to an Nd removal efficiency of approximately 96% based on mass balance. These results demonstrate that HbetCl can efficiently and selectively dissolve Nd_2O_3 from the UO_2-based simulated spent fuel matrix, enabling effective lanthanide removal while preserving the actinide oxide residue.

To recover dissolved neodymium from the Nd-loaded HbetCl solution, solid oxalic acid was introduced to precipitate rare earth elements in the form of oxalate precipitates [37]. After that, the Nd-oxalated precipitate obtained was separated from HbetCl and calcinated at 800 °C for 3 h. X-ray diffraction (XRD) analysis confirmed that the obtained oxide was Nd_2O_3 (Figure S3), further demonstrating the feasibility of selectively leaching Nd_2O_3 from the UO_2 fuel matrix. Moreover, inductively coupled plasma–optical emission spectrometry (ICP-OES) measurements showed that the recovery efficiency of Nd from HbetCl via oxalic acid precipitation could reach 99%. As an essential secondary purification step, oxalate precipitation achieves effective separation of lanthanides and co-dissolved uranium. Under the optimized precipitation conditions, lanthanide ions are completely precipitated as oxalate precursors, while the co-dissolved uranium predominantly remains in the aqueous solution in the form of uranyl species.

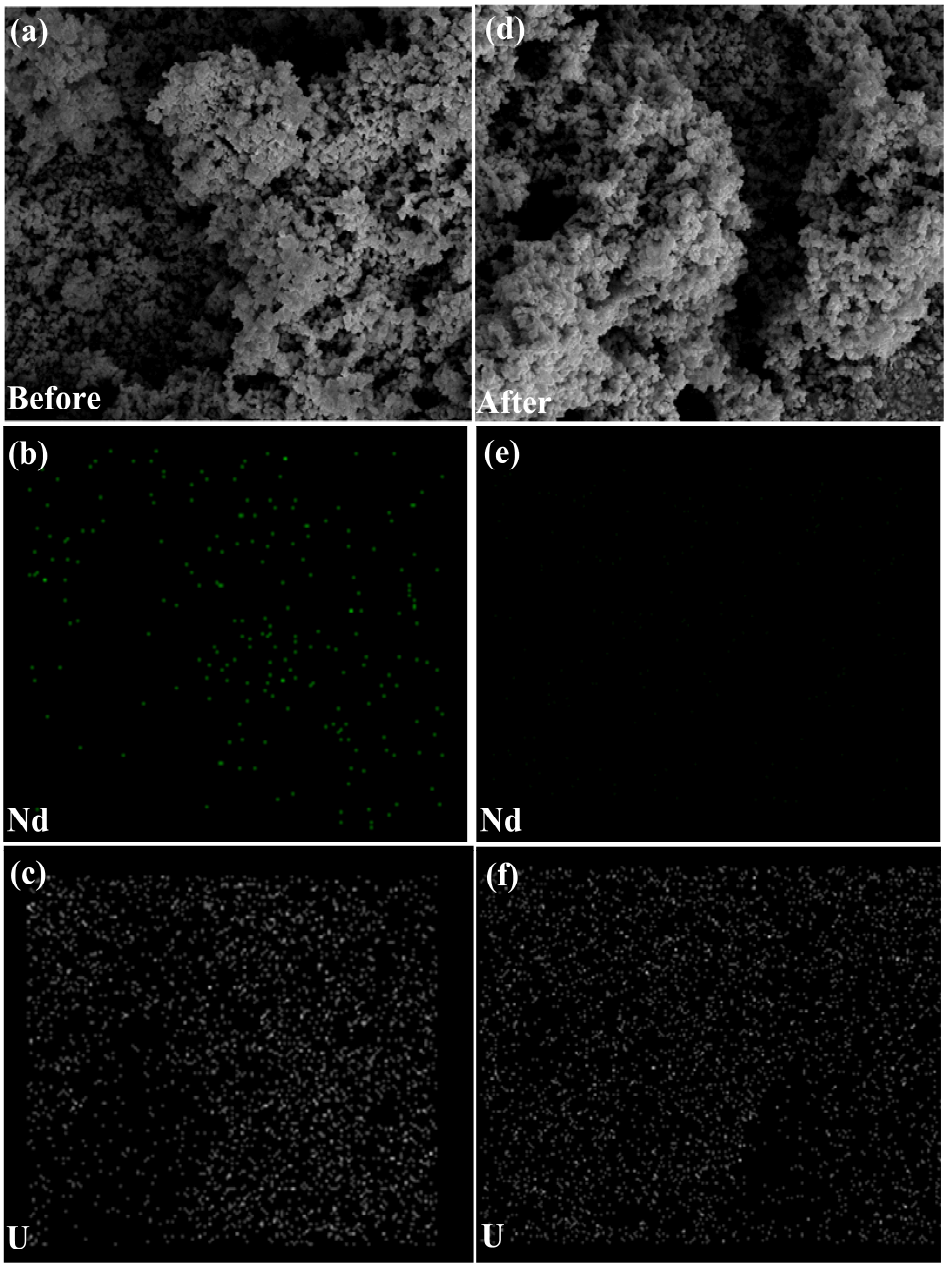


Figure 5. SEM images and EDS elemental maps of SIMFUEL before and after selective dissolution in aqueous HbetCl: (**a**,**d**) SEM images; (**b**,**e**) Nd elemental maps; and (**c**,**f**) U elemental maps. Panels (**a**–**c**) show the sample before dissolution, whereas panels (**d**–**f**) show the solid residue after dissolution.

3.2. Dissolution Mechanism

To elucidate the dissolution mechanism and the complexation behavior between HbetCl and Nd^{3+}, various characterization approaches were adopted to investigate the Nd-loaded HbetCl system after dissolution. FTIR spectroscopy is often used to elucidate the molecular structure due to the vibrational spectrum can reflect well the characteristics of a molecule [38]. As shown in Figure 6, the change of FTIR spectra after the dissolution of Nd confirmed the interaction between HbetCl and Nd_2O_3. Given that HbetCl dissociates into $Hbet^+$ and Cl^- in aqueous solution, the dissolution products of HCl with Nd_2O_3 and commercial $NdCl_3$ were also examined for comparison, to assess the potential role of Cl^- in complexation with Nd^{3+}. In the FTIR spectrum of pure HbetCl, the band at 1728 cm^{-1} is attributed to the carboxylate (COO^-) group [39,40]. After dissolution, a shift of the vibration of COO^- to lower wavenumbers and two low intensity bands can be observed at 1656 cm^{-1} and 1591 cm^{-1}, which suggests the carboxylate group to the metal atom Nd. In the aqueous solution of HbetCl, $Hbet^+$ undergoes hydrolysis to release H^+, which promotes the dissolution of Nd_2O_3 and facilitates the formation of coordination bonds with COO^-. Moreover, IR spectroscopy shows that the bands positions of $NdCl_3$ and Nd-loaded HbetCl are similar, but

not identical, implying the possible coordination of chloride to Nd^{3+}. As chloride is known to act as an inner-sphere ligand, it is plausible that extractable chlorometallate complexes are formed in the system [41].

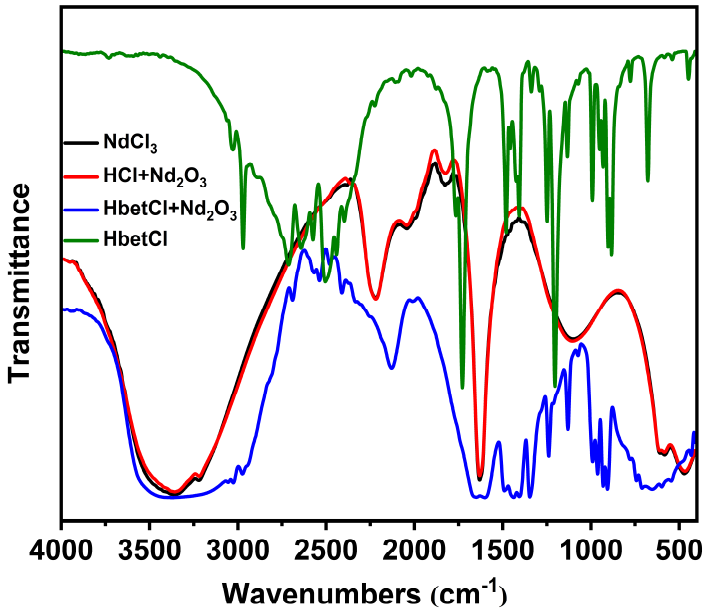


Figure 6. FTIR spectra of HBetCl, $NdCl_3$ and Nd_2O_3 dissolved in HBetCl and HCl.

Furthermore, the UV-Vis spectra of Nd^{3+} were analyzed to explore its coordination environment in the HbetCl solution. As displayed in Figure 7, the characteristic absorption band of Nd^{3+} shifted from 575 nm to 577 nm when HbetCl was utilized as the dissolution agent. According to the literature [42,43], the absorption band of Nd^{3+} at around 575 nm is highly sensitive to changes in its coordination environment. The minor difference observed in the absorption bands between Solution 1 (Nd_2O_3 dissolved in HCl) and Solution 2 (Nd_2O_3 dissolved in HbetCl) indicates a similar coordination environment for Nd^{3+} in both systems. In the HbetCl system, it can be inferred that Nd^{3+} coordinates not only with the Bet^- generated in the aqueous solution but also with Cl^-, which accounts for this slight spectral shift. Previous studies have also revealed that Nd cations coordinate with Cl^- to form complex anions in ionic liquids and deep eutectic solvents (DESs) [29,44,45]. Combined with the literature and our spectroscopic analysis, it can be deduced that the dissolution of Nd_2O_3 fundamentally relies on both the acidity of the -COOH group in HbetCl and the synergistic coordination capability of Cl^- and Bet^-. To explicitly validate the acid-dependent mechanism and address the consumption of protons during the process, the pH of the solution was monitored. The initial pH of the HbetCl solution was measured at 0.79, which increased to 0.88 following the dissolution of Nd_2O_3. The pH value of 0.79 indicates that in the 1 M betaine hydrochloride (HbetCl) solution, the $-COO^-$ group of betaine predominantly exists in its protonated form (-COOH). Furthermore, the pronounced acid consumption observed following the dissolution confirms that protons from the carboxyl group (-COOH) actively participate in and drive the dissolution reaction. Moreover, under identical experimental conditions, a significantly higher solubility of Nd_2O_3 was observed in 1 M HbetCl (98 $g \cdot L^{-1}$) compared to 1 M HCl (37 $g \cdot L^{-1}$). This enhanced solubility can be attributed to the dual coordination of Bet^- and Cl^- with Nd^{3+} in the HbetCl solution, which facilitates dissolution likely via the formation of soluble $[Nd(H_2O)_6Cl_3](bet)_X$ complex species. Consequently, it can be concluded that the dissolution of Nd_2O_3 in the HbetCl solution proceeds according to the following reaction, which exhibits mechanistic similarities to its dissolution in HCl.

$$Nd_2O_3 + 6HbetCl + 9H_2O = 2[Nd(H_2O)_6Cl_3](bet)_X + (6 - 2X)bet$$

To further elucidate the role of betaine during the dissolution process, density functional theory (DFT) calculations were performed to model the Nd(III)-containing complexes. The optimized structures in Figure 8 compare three Nd(III)-chloride aqua complexes: the reference $[Nd(H_2O)_6Cl_3]$ cluster, the betaine-associated complex $[Nd(H_2O)_6Cl_3]bet$, and the water-associated complex $[Nd(H_2O)_6Cl_3]H_2O$. In all models, Nd is located at the coordination center and is surrounded by water molecules and chloride ions, while betaine remains outside the first coordination sphere and interacts mainly through its carboxylate group. The DFT results show that the binding energy of $[Nd(H_2O)_6Cl_3]$ is −97.85 kJ/mol, whereas the introduction of one betaine molecule markedly decreases the energy to −101.43 kJ/mol, indicating a more thermodynamically stable supramolecular complex. This calculated stabilization is consistent with the experimental solubility results summarized in Table 1. This

stabilization can be attributed to the two strong hydrogen bonds formed between the carboxylate oxygen atoms of betaine and the hydrogen atoms of neighboring coordinated water molecules, with H···O distances of 1.611 and 1.619 Å [46]. In contrast, adding an extra water molecule leads to a binding energy of only −97.78 kJ/mol for $[Nd(H_2O)_6Cl_3]H_2O$. This result indicates that external water does not provide comparable stabilization because its hydrogen-bonding interaction with the Nd aqua-chloro cluster is weaker and less directional than the carboxylate-mediated interaction of betaine. This interpretation is also consistent with broader lanthanide chemistry: Nd(III) in chloride-containing aqueous systems readily forms aqua-chloroaqua complexes, and the stability and mobility of rare-earth ions are strongly controlled by ligand complexation in solution [47], and organic ligands containing carboxylate groups are particularly effective in stabilizing Ln(III) species through coordination or secondary-sphere interactions [48,49]. Therefore, the calculated energy trend and hydrogen-bond geometry together indicate that betaine acts as a secondary-sphere stabilizer of the $[Nd(H_2O)_6Cl_3]$ complex, which can facilitate Nd_2O_3 dissolution by stabilizing dissolved Nd(III)-containing species, whereas water alone is insufficient to produce the same stabilizing effect.

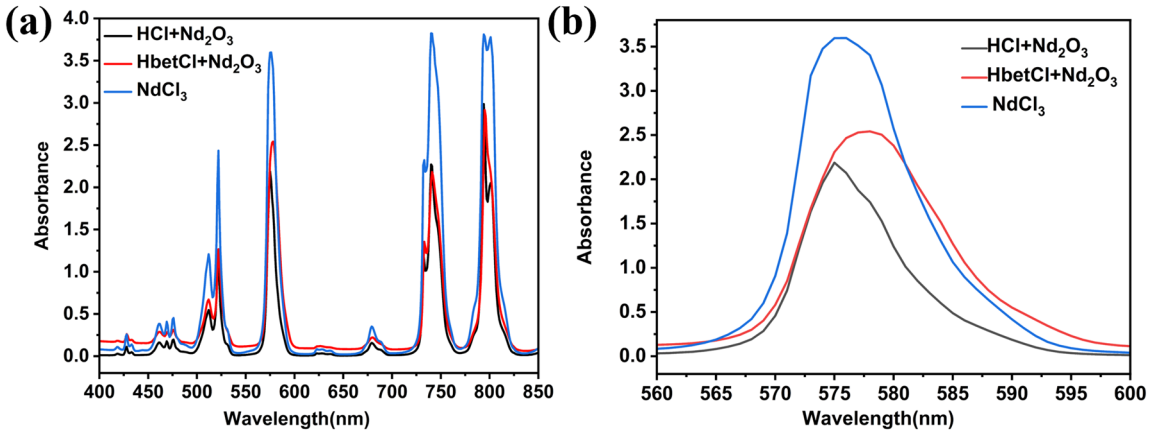


Figure 7. UV-Vis absorption spectra of the $NdCl_3$ reference solution and the solutions obtained by dissolving Nd_2O_3 in HCl or HbetCl: (**a**) spectra over 400–850 nm; (**b**) enlarged view of the 560–600 nm region.

Table 1. Solubility of Nd_2O_3 in HbetCl solution (1 M, 2 mL) and HCl (1 M, 2 mL).

Complexes	Solubility (g/L)	Binding Energy (kJ/mol)
$[Nd(H_2O)_6Cl_3]$	74.09	−97.85
$[Nd(H_2O)_6Cl_3]$bet	98.02	−101.43

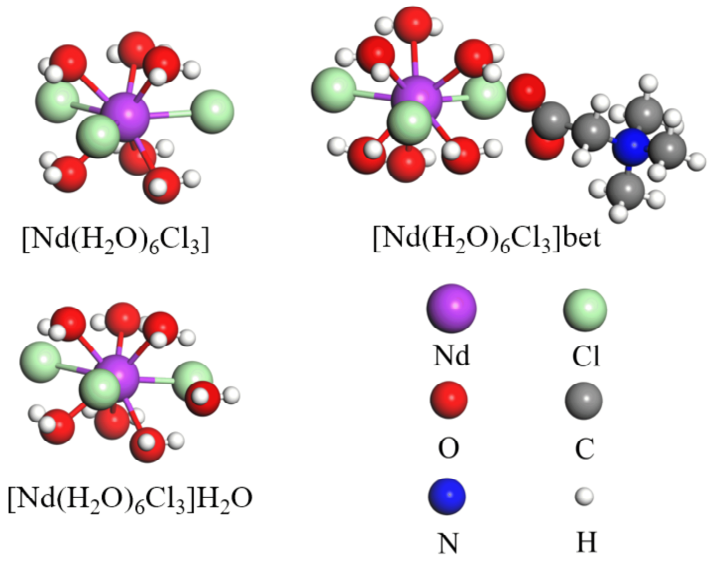


Figure 8. Overview of optimized aqueous Nd complexes.

3.3. Selective Dissolution of Mixed Lanthanides from Simulated Spent Nuclear Fuel

Inspired by Nd dissolution separation in the biphasic system of Nd_2O_3/UO_2 sample, we pursued this approach for mixed lanthanides separation from simulated spent fuel sample using HbetCl solution. The sample was sintered at 1000 °C, and the contents of Nd, Sm, Eu, Gd were 5.34 wt%, 5.8 wt%, 6.28 wt% and 6.33 wt%, respectively. As shown in Figure 9, HbetCl retains superior dissolution activity towards lanthanides in these simulated spent fuel samples. The separation of multiple coexist Ln_2O_3 under the same conditions are almost identical to single Nd_2O_3 from simulated spent nuclear fuel. Notably, all measured dissolution efficiency of Nd, Sm, Eu, Gd can reach over 95%, whereas the dissolution efficiency of U is only 1.11%. The results indicate that betaine hydrochloride could highly-selectively dissolve Ln_2O_3. Therefore, we established a selective leaching process for separation of lanthanides and recovery of actinides, aiming to achieve a simple and green recycle process for spent nuclear fuel.

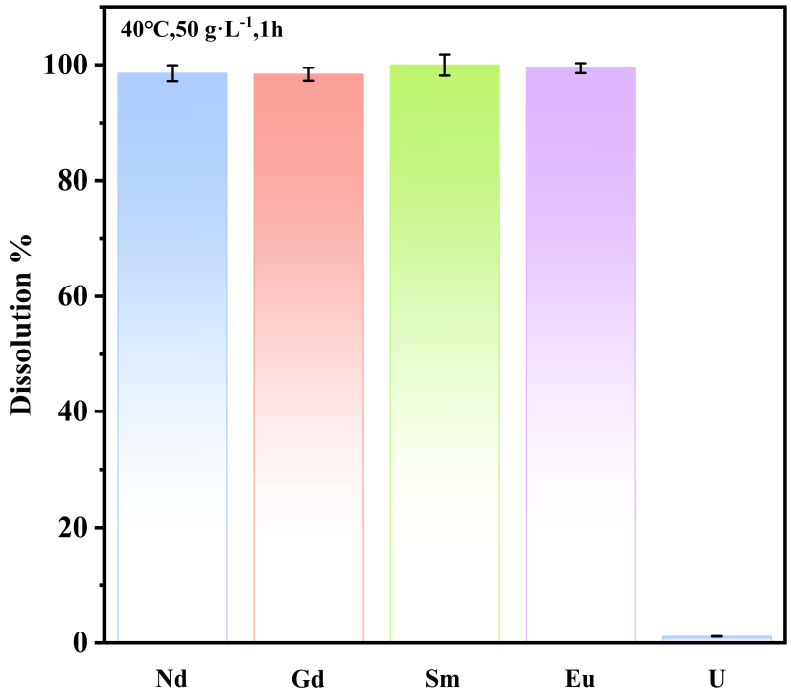


Figure 9. Dissolution efficiency of UO_2 and Ln_2O_3 from simulated spent nuclear fuel.

3.4. Selective Separation and Recovery of Group Actinides

To further test the utility of this novel selective dissolution separation strategy for spent nuclear fuel reprocessing, the dissolution ability of several representative fission products in HbetCl solution was also investigated. The solubility data of these metal oxides are summarized in Table 2. The experimental results are in good agreement with our prior work [28], indicating that metal oxides exhibit similar dissolution trends in [Hbet][Tf_2N] and in HbetCl solution. Obviously, HbetCl exhibits a remarkable dissolution ability towards M_2O_3-type and MO-type metal oxides, while displaying much lower solubility for MO_2-type compounds. This difference could be attributed to the weaker M-O bonding, lower lattice energy, and higher acid reactivity of M_2O_3 and MO oxides compared to their MO_2 counterparts. Therefore, the low solubility of MO_2-type metal oxides such as UO_2 and ThO_2 in HbetCl gives an opportunity to achieve group separation and recovery of uranium and transuranic elements via selective dissolution.

Table 2. Solubility of some fission products in HbetCl solution (1 M, 2 mL) and the corresponding *U/x* values (in kJ/mol) calculated from the lattice energy data. The dissolution time and temperature were 60 min and 25 °C, respectively.

M_2O_3	Solubility (g/L)	*U/x* (kJ/mol)	MO_2	Solubility (g/L)	*U/x* (kJ/mol)	MO	Solubility (g/L)	*U/x* (kJ/mol)
La_2O_3	52.85	6189	UO_2	0.52	10682	SrO	29.2	3322
Pr_2O_3	55.15	6322	$^{243}AmO_2$	0.006	10540	BaO	50.65	3116
Nd_2O_3	98.02	6929	ThO_2	0.35	10147	CdO	32.13	3657
Sm_2O_3	79.98	6417						
Eu_2O_3	117.5	6469						
Gd_2O_3	76.4	6400						

In this study, the dissolution experiment of $^{243}AmO_2$ demonstrated that HbetCl exhibits only negligible dissolving ability toward americium dioxide, further supporting the feasibility of solid-phase group recovery of actinide dioxides during selective lanthanide dissolution. Americium was selected as a representative minor actinide because it is generated in nuclear reactors through neutron-capture processes and constitutes one of the most important long-lived actinides in spent nuclear fuel. In particular, Am isotopes are major contributors to the long-term radiotoxicity and decay heat of high-level radioactive waste, and their management is a central issue in advanced fuel-cycle strategies involving partitioning and transmutation. Therefore, investigating the dissolution behavior of AmO_2 is important for evaluating whether the HbetCl system can selectively dissolve lanthanide oxides while retaining both major and minor actinide dioxides in the solid phase [50,51]. Americium is a neutron-capture by-product of nuclear power generation and a major contributor to the long-term radiotoxicity of high-level waste [52,53]. The apparent dissolved concentration of $^{243}AmO_2$ in 1 M HbetCl was determined by HPGe gamma spectrometry. Before dissolution, the activity of approximately 0.12 mg of $^{243}AmO_2$ (0.82 MBq) was measured. The solid was subsequently contacted with 2 mL of 1 M HbetCl at 25 °C under stirring for 60 min. Because of the extremely small sample mass and high specific radioactivity, conventional centrifugation was not employed; instead, the suspension was allowed to stand overnight to obtain clear phase separation. A 100 μL aliquot of the supernatant was then withdrawn and measured by HPGe γ-ray spectrometry using the same calibrated counting geometry. After background correction, the dissolved fraction of AmO_2 was quantified according to the measured radioactivity. The calculated solubility of AmO_2 was 6.31 mg/L, which is substantially lower than the 0.52 g/L solubility of UO_2 tested under identical conditions. The corresponding γ-ray spectra are shown in Figure 10. This low solubility implies that AmO_2 remained almost entirely in the solid phase, supporting the feasibility of group recovery of actinide dioxides. In addition, gamma-ray spectroscopic analysis of the $^{243}AmO_2$ solid clearly distinguished characteristic peaks of ^{239}Np, which is the radioactive decay progeny of ^{243}Am. Trace indigenous Np was confirmed in the solid lattice of AmO_2. The in-situ radiogenic ^{239}Np exhibited dissolution behavior consistent with its parent Am, demonstrating the inherently low solubility of tetravalent NpO_2. Because the total time (≈6 h) for dissolution equilibration and radiometric measurement was much shorter than the short half-life of ^{239}Np (t≈2.4 days), the radioactive decay of Np during the experiment was negligible and did not interfere with the measurement results. Hence, HbetCl shows negligible dissolving ability toward minor actinide oxides under the experimental conditions applied. These results confirm the potential of HbetCl-based selective dissolution for the solid-phase group recovery of actinide dioxides (AnO_2) during spent-fuel reprocessing.

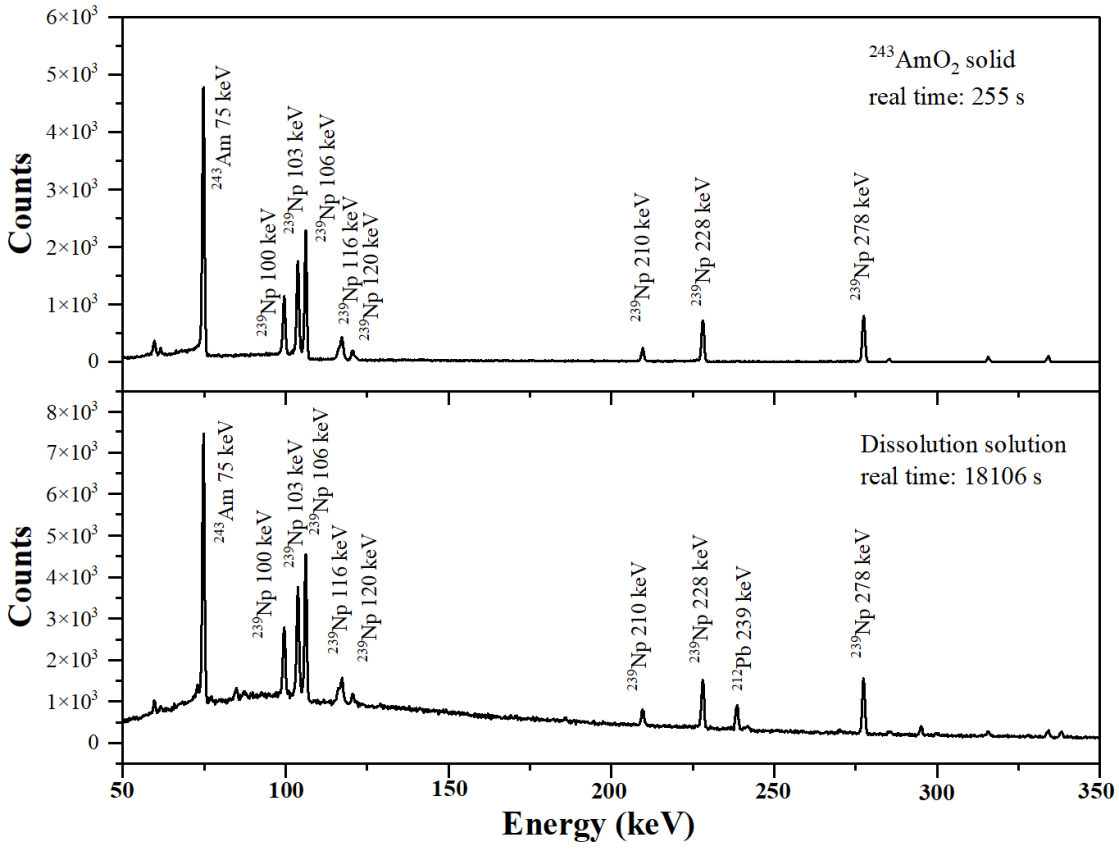


Figure 10. The γ spectra of ^{243}Am.

Similarly, the solubility of these metal oxides in HbetCl was clarified using the lattice energy *U* [54], which has been utilized to estimate the dissolution propensity of metal oxides in related reports [55]. The lattice energy *U* for all evaluated metal oxides was calculated [28], and the corresponding *U*/*x* values are listed in Table 2. Rather than following a strict linear relationship with lattice energy across all oxides, the data reveal a threshold-governed behavior. Specifically, metal oxides with a *U*/*x* value exceeding 10,000 kJ/mol (such as the MO_2-type oxides) exhibit negligible solubility and remain almost entirely insoluble. In contrast, oxides with *U*/*x* values well below this threshold (like lanthanide sesquioxides) and MO-type oxides exhibit significantly higher solubility. This macroscopic trend is thermodynamically consistent. The disruption of the crystalline lattice constitutes the essential initial step in dissolution, and the considerable energy required to break the strong lattice of MO_2 oxides severely limits their dissolution. This provides a clear thermodynamic foundation for the high selectivity observed in the dissolution process.

3.5. Radiolytic Stability Studies

Although HbetCl demonstrates high potential for lanthanide separation and actinide recovery, its practical applicability in spent nuclear fuel reprocessing depends critically on its radiolytic stability [53]. Here, the radiolytic degradation studies of HbetCl was evaluated using a ^{60}Co γ-irradiator. After irradiation, the HbetCl samples were measured by means of several analytical techniques. Both FTIR and UV-Vis spectra (Figures S5 and S6) of samples subjected to accumulated absorbed doses ranging from 100 to 1000 kGy showed that the original molecular structure remained essentially unchanged, indicating excellent radiolytic stability over a wide dose range. Furthermore, the stability of HbetCl is confirmed by the ESI-MS data, in which no changes to the solution pattern are apparent before and after irradiation (Figure 11). The designation of signals for the samples are summarized in Table 3. These results stand in sharp contrast to earlier reports on the ionic liquid [Hbet][Tf_2N], which undergoes significant radiolytic degradation under similar conditions, despite sharing the same $[Hbet]^+$ cation. In the case of [Hbet][Tf_2N], irradiation produced new signals in the ESI-MS spectra, indicating fragmentation of the ionic liquid. However, even at 1000 kGy γ-irradiation, HbetCl exhibited no detectable degradation, and no new signals emerged in the ESI-MS spectra compared with the unirradiated sample. As a consequence, it can be deduced that the anions can positively influence the stability of cation $[Hbet]^+$. Overall, HbetCl exhibits excellent radiolytic stability with no observable radiation-induced degradation up to 1000 kGy. Such excellent radiation stability further sheds light on the value and great potential of HbetCl as a promising medium for lanthanides in the field of spent nuclear fuel reprocessing.

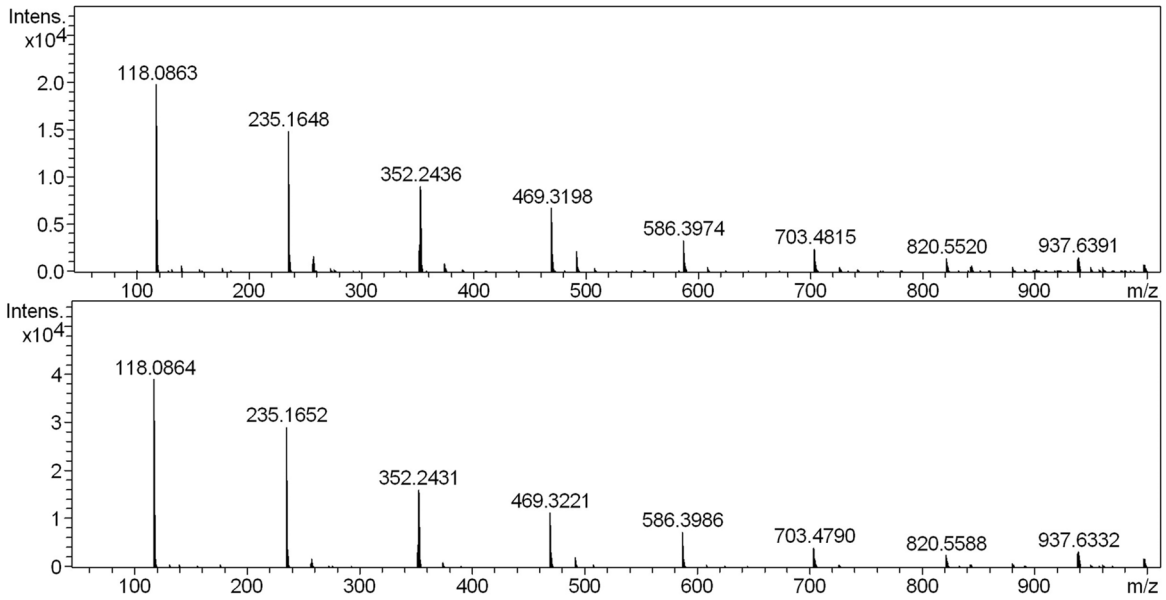


Figure 11. ESI-MS spectra in positive ionization mode of HbetCl before (**upper**) and after (**down**) irradiation at 1000 kGy.

To further explore the practical applicability, HbetCl samples that had been irradiated to different cumulative absorbed doses were employed for the separation of lanthanide oxides from simulated spent fuel. As demonstrated in Figure 12, the dissolution selectivity and performance of HbetCl toward lanthanides remained essentially unchanged after irradiation. Remarkably, HbetCl was still able to selectively remove nearly 96% of Nd from the

simulated spent fuel even after exposure to high dose (1000 kGy) of radiation. However, previous work reported that the ionic liquid [Hbet][Tf_2N] suffers from poor radiolytic stability, and its dissolution efficiency for Nd_2O_3 is significantly affected by radiation dose. It should be noted that solid HbetCl was irradiated firstly and then dissolved into water to prepare the separation medium. Because a 1 M HbetCl solution was used in all separation experiments, the dissolution performance was also evaluated directly using 1 M HbetCl solution that had been irradiated in liquid form (Figure S7). Obviously, the results obtained with irradiated solid and irradiated solution were nearly identical, indicating that HbetCl retains its lanthanide-separation capability regardless of the irradiation state. These observations are consistent with the conclusion that no radiation degradation under gamma irradiation observed in the ESI-MS spectra. Based on the preserved selectivity toward Nd_2O_3 after irradiation, we believe that HbetCl shows promising potential for separation applications within the nuclear fuel cycle. In addition, and importantly, irradiation of HbetCl does not alter its dissolution behavior toward uranium. The dissolution efficiency of UO_2 remained consistently low (~1%), confirming that HbetCl maintains a strong and distinct preference for Nd_2O_3 over UO_2. Therefore, such a unique property endows that HbetCl is an extremely attractive candidate to simultaneously separate lanthanides oxide and recover actinides from spent nuclear fuel.

Table 3. Designation of signals of HbetCl before and after γ-irradiation.

Num.	Experimental *m*/*z*	Designation	Theoretical *m*/*z*
1	118.0889	$[Hbet]^+$	118.0863
2	235.1653	$[[Hbet]\ [bet]]^+$	235.1652
3	352.2425	$[[Hbet]\ [bet]_2]^+$	352.2442
4	469.3231	$[[Hbet]\ [bet]_3]^+$	469.3232
5	586.4029	$[[Hbet]\ [bet]_4]^+$	586.4022
6	703.4746	$[[Hbet]\ [bet]_5]^+$	703.4811
7	820.5561	$[[Hbet]\ [bet]_6]^+$	820.5601
8	937.6344	$[[Hbet]\ [bet]_7]^+$	937.6325

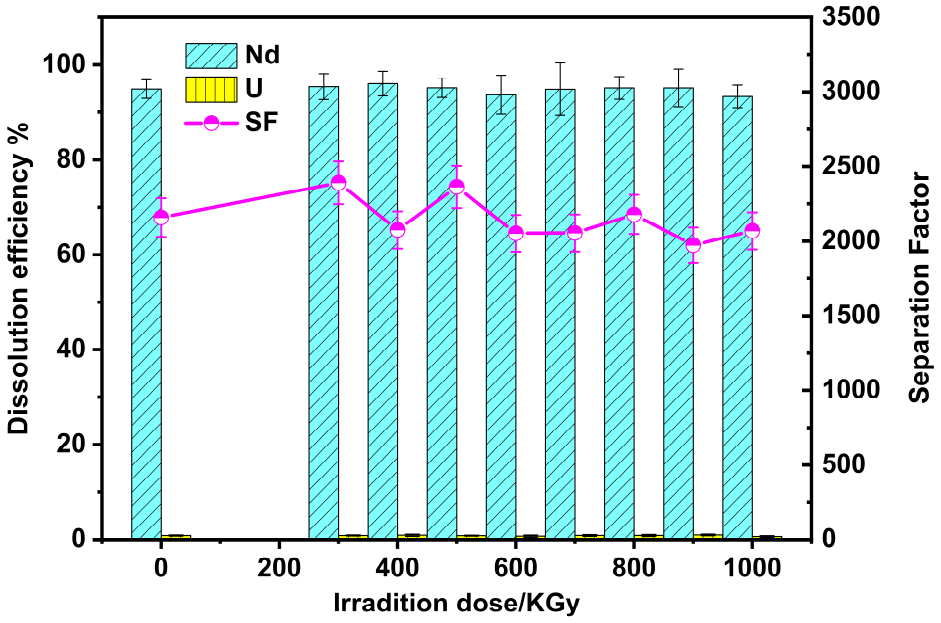


Figure 12. Influence of HbetCl with different accumulative absorbed doses on the dissolution of Nd_2O_3 and UO_2 from simulated nuclear fuel.

Finally, we compared the present system with previously reported systems [28,56] around the following aspects. (1) Dissolution selectivity: Both systems exhibit the same overall dissolution pattern, preferentially dissolving Ln_2O_3 while retaining most UO_2 and other AnO_2-type oxides in the solid phase. Under comparable conditions (40 °C, 60 min, solid-to-liquid ratio of 50 $g \cdot L^{-1}$), both media achieve lanthanide dissolution rates exceeding 95% with UO_2 dissolution limited to approximately 1%. (2) Coordination environment: The two media stabilize dissolved Ln^{3+} through fundamentally different coordination modes. In aqueous HbetCl, Cl^- acts as an inner-sphere ligand forming aqua-chloro complexes, while betaine provides outer-sphere stabilization via hydrogen bonding. In [Hbet][Tf_2N], betaine coordinates more directly with Ln^{3+}, whereas the bulky, charge-delocalized, and weakly coordinating Tf_2N^- serves primarily as a counter anion governing the hydrophobicity and

phase behavior of the ionic liquid. (3) Radiation resistance: HbetCl retains its selective dissolution performance up to 1000 kGy with no detectable degradation, whereas [Hbet][Tf_2N] shows a marked decline in dissolution efficiency above approximately 300 kGy. This difference is of particular importance for applications involving highly radioactive materials. (4) Potential applications: HbetCl offers direct aqueous preparation from a commercially available salt, avoids fluorinated reagents, and is compatible with existing aqueous processing infrastructure. In contrast, [Hbet][Tf_2N] requires multi-step synthesis, purification, and water-content adjustment prior to use. Based on the above comparison, HbetCl appears better suited for large-scale or high-dose applications where operational simplicity, cost, and radiation stability are critical.

4. Conclusions

In this manuscript, radiation-resistant betaine hydrochloride (HbetCl) was demonstrated as an additive-free and operationally simple medium for facile Ln/An group separation from simulated spent nuclear fuel via selective dissolution. Owing to its distinct dissolution selectivity, HbetCl preferentially dissolved more than 95% of Ln_2O_3, while UO_2 and AmO_2-type actinide dioxides remained nearly insoluble. This phase-selective behavior enabled lanthanides to be transferred into the aqueous phase and actinide dioxides to be preserved as solid residues, providing a straightforward route for Ln/An group separation through simple solid–liquid separation. A closed separation and recovery route was further demonstrated. After selective dissolution, the dissolved lanthanides were efficiently recovered as high-purity Ln_2O_3 through oxalic acid precipitation followed by calcination. Meanwhile, the undissolved AnO_2-type oxides remained as solid residues, supporting the feasibility of simultaneous lanthanide recovery and actinide dioxide retention within one integrated process. This dissolution-precipitation-calcination sequence confirms that HbetCl can serve not only as a selective dissolution medium but also as a practical platform for downstream lanthanide recovery. The stability of HbetCl under ionizing radiation was also verified. After exposure to γ-radiation doses up to 1000 kGy, HbetCl retained its selective dissolution performance and was still able to remove nearly 97% of Nd from simulated spent fuel. This excellent radiation tolerance is particularly important for potential applications in spent-fuel treatment, where the dissolution medium is inevitably exposed to intense radiation fields. The origin of the selective dissolution behavior was further clarified by experimental observations and theoretical calculations. The distinct dissolution tendencies of Ln_2O_3 and AnO_2 are mainly associated with the different lattice energies required to disrupt their corresponding metal–oxygen frameworks. Compared with Ln_2O_3, AnO_2-type oxides possess more robust oxide lattices, which accounts for their much lower dissolution in HbetCl solution. In addition, DFT simulations revealed that betaine can interact with lanthanide-containing species through hydrogen-bonding interactions, thereby stabilizing dissolved lanthanide species and thermodynamically facilitating the dissolution of lanthanide oxides. Overall, this work establishes an additive-free and operationally simple selective dissolution strategy for separating lanthanides from actinides in simulated spent nuclear fuel. By transferring lanthanides into solution while keeping actinide dioxides in the solid phase, this approach avoids reliance on conventional large-volume liquid–liquid extraction processes and may help reduce the generation of high-level radioactive liquid waste. These advantages, together with the easy availability of HbetCl and its effective dissolution performance toward selected metal oxides, suggest promising potential not only for advanced spent-fuel reprocessing but also for hazardous solid waste treatment and rare-earth recovery from end-of-life products and industrial waste streams.

Supplementary Materials

The additional data and information can be downloaded at: https://media.sciltp.com/articles/others/2611020909309905/MNR-26070067-SM-FC-done.pdf. Figure S1. The XRD pattern of SIMFUEL. Figure S2. The dissolution of Nd_2O_3, UO_2 and U_3O_8 in HbetCl aqueous. Figure S3. The XRD diagram of Nd_2O_3 and $Nd_2(C_2O_4)_3{\cdot}10H_2O$. Figure S4. Effects of heat-treatment temperature and dissolution time on the dissolution efficiencies of (a) Nd_2O_3 and (b) UO_2 from SIMFUEL in 1 M aqueous HbetCl at 40 °C. The solid: liquid ratio is 50 mg/mL. Figure S5. FT-IR spectra of HbetCl samples before and after γ-irradiation. Figure S6. UV-Vis spectra of HbetCl solution before and after irradiation. Figure S7. Influence of HbetCl with different accumulative absorbed doses on the dissolution of Nd_2O_3 and UO_2 from simulated nuclear fuel. The solid: liquid ratio is 50 mg/mL. 1 M HbetCl solution was irradiated directly.

Author Contributions

Z.-F.J.: writing—original draft, formal analysis, data curation; H.-X.J.: data curation; B.-Q.W.: writing—review & editing, data curation, formal analysis; Q.-G.H.: validation; D.-S.C.: resources; X.-J.Y.: resources; S.-W.C.:

resources; Z.Q.: resources, supervision, funding acquisition; F.-L.F.: writing—review & editing, writing—original draft, validation, supervision, funding acquisition. All authors have read and agreed to the published version of the manuscript.

Funding

This work was supported by the National Natural Science Foundation of China (No. 22276196) and the Natural Sciences Foundation of Gansu Province (No. 22JR5RA120).

Institutional Review Board Statement

Not applicable. This study did not involve humans or animals.

Informed Consent Statement

Not applicable.

Data Availability Statement

The data supporting the findings of this study are presented in the article and its Supplementary Materials. Additional data are available from the corresponding author upon reasonable request.

Conflicts of Interest

The authors declare no conflict of interest.

Use of AI and AI-Assisted Technologies

During the preparation of this work, the authors used ChatGPT (OpenAI) to assist with language polishing. After using this tool, the authors reviewed and edited the content as needed and take full responsibility for the content of the published article.

References

1. Pateli, I.M.; Thompson, D.; Alabdullah, S.S.M.; et al. The Effect of pH and Hydrogen Bond Donor on the Dissolution of Metal Oxides in Deep Eutectic Solvents. *Green Chem.* **2020**, *22*, 5476–5486. https://doi.org/10.1039/d0gc02023k.
2. Chen, W.; Jiang, J.; Lan, X.; et al. A Strategy for the Dissolution and Separation of Rare Earth Oxides by Novel Brønsted Acidic Deep Eutectic Solvents. *Green Chem.* **2019**, *21*, 4748–4756. https://doi.org/10.1039/c9gc00944b.
3. Binnemans, K.; Jones, P.T. Solvometallurgy: An Emerging Branch of Extractive Metallurgy. *J. Sustain. Metall.* **2017**, *3*, 570–600. https://doi.org/10.1007/s40831-017-0128-2.
4. Meshram, P.; Mishra, A.; Abhilash; et al. Environmental Impact of Spent Lithium Ion Batteries and Green Recycling Perspectives by Organic Acids—A Review. *Chemosphere* **2020**, *242*, 125291. https://doi.org/10.1016/j.chemosphere.2019.125291.
5. Xie, F.; Zhang, T.A.; Dreisinger, D.; et al. A Critical Review on Solvent Extraction of Rare Earths from Aqueous Solutions. *Miner. Eng.* **2014**, *56*, 10–28. https://doi.org/10.1016/j.mineng.2013.10.021.
6. Leoncini, A.; Huskens, J.; Verboom, W. Ligands for F-Element Extraction Used in the Nuclear Fuel Cycle. *Chem. Soc. Rev.* **2017**, *46*, 7229–7273. https://doi.org/10.1039/c7cs00574a.
7. Mattocks, J.A.; Cotruvo, J.A. Biological, Biomolecular, and Bio-Inspired Strategies for Detection, Extraction, and Separations of Lanthanides and Actinides. *Chem. Soc. Rev.* **2020**, *49*, 8315–8334. https://doi.org/10.1039/d0cs00653j.
8. Kolarik, Z. Complexation and Separation of Lanthanides(III) and Actinides(III) by Heterocyclic N-Donors in Solutions. *Chem. Rev.* **2008**, *108*, 4208–4252. https://doi.org/10.1021/cr078003i.
9. Gunarathne, V.; Rajapaksha, A.U.; Vithanage, M.; et al. Hydrometallurgical Processes for Heavy Metals Recovery from Industrial Sludges. *Crit. Rev. Environ. Sci. Technol.* **2022**, *52*, 1022–1062. https://doi.org/10.1080/10643389.2020.1847949.
10. Jung, J.C.Y.; Sui, P.C.; Zhang, J. A Review of Recycling Spent Lithium-Ion Battery Cathode Materials Using Hydrometallurgical Treatments. *J. Energy Storage* **2021**, *35*, 102217. https://doi.org/10.1016/j.est.2020.102217.
11. Verma, P.K.; Mahanty, B.; Sengupta, A.; et al. Simple, Fast, and Selective Dissolution of Eu_2O_3 in an Ionic Liquid as a Sustainable Paradigm for Lanthanide–Actinide Separations in Radioactive Waste Remediation. *Inorg. Chem.* **2023**, *62*, 87–97. https://doi.org/10.1021/acs.inorgchem.2c02965.
12. Gao, X.; Ding, A.; Li, Y.; et al. Selective Dissolution and Separation of Lanthanides and Actinides from Spent Nuclear Fuel Using Inorganic Salt Solutions: A Sustainable Approach. *Sep. Purif. Technol.* **2025**, *360*, 131035. https://doi.org/10.1016/j.seppur.2024.131035.

13. Collins, E.; DelCul, G.; Spencer, B.; et al. *State-of-the-Art Report on the Progress of Nuclear Fuel Cycle Chemistry*; OECD Publishing: Paris, France, 2018. https://doi.org/10.1787/9789264298545-en.
14. Baron, P.; Cornet, S.M.; Collins, E.D.; et al. A Review of Separation Processes Proposed for Advanced Fuel Cycles Based on Technology Readiness Level Assessments. *Prog. Nucl. Energy* **2019**, *117*, 103091. https://doi.org/10.1016/j.pnucene.2019.103091.
15. Yan, X.; Yang, L.; Zhang, X.; et al. Concept of an Accelerator-Driven Advanced Nuclear Energy System. *Energies* **2017**, *10*, 944. https://doi.org/10.3390/en10070944.
16. George, K.; Masters, A.J.; Livens, F.R.; et al. A Review of Technetium and Zirconium Extraction into Tributyl Phosphate in the PUREX Process. *Hydrometallurgy* **2022**, *211*, 105892. https://doi.org/10.1016/j.hydromet.2022.105892.
17. Taylor, R.; Mathers, G.; Banford, A. The Development of Future Options for Aqueous Recycling of Spent Nuclear Fuels. *Prog. Nucl. Energy* **2023**, *164*, 104837. https://doi.org/10.1016/j.pnucene.2023.104837.
18. Dupont, D.; Binnemans, K. Rare-Earth Recycling Using a Functionalized Ionic Liquid for the Selective Dissolution and Revalorization of Y_2O_3:Eu^{3+} from Lamp Phosphor Waste. *Green Chem.* **2015**, *17*, 856–868. https://doi.org/10.1039/c4gc02107j.
19. Liu, Y.C.; Liu, Y.L.; Zhao, Y.; et al. A Simple and Effective Separation of UO_2 and Ln_2O_3 Assisted by NH_4Cl in LiCl–KCl Eutectic. *J. Nucl. Mater.* **2020**, *532*, 152049. https://doi.org/10.1016/j.jnucmat.2020.152049.
20. Van Loy, S.; Binnemans, K.; Van Gerven, T. Mechanochemical-Assisted Leaching of Lamp Phosphors: A Green Engineering Approach for Rare-Earth Recovery. *Engineering* **2018**, *4*, 398–405. https://doi.org/10.1016/j.eng.2018.05.015.
21. Venkatesan, P.; Vander Hoogerstraete, T.; Hennebel, T.; et al. Selective Electrochemical Extraction of REEs from NdFeB Magnet Waste at Room Temperature. *Green Chem.* **2018**, *20*, 1065–1073. https://doi.org/10.1039/c7gc03296j.
22. Journoux-Lapp, C.; De Oliveira Vigier, K.; Bachmann, C.; et al. Elucidation of the Role of Betaine Hydrochloride in Glycerol Esterification: Towards Bio-Based Ionic Building Blocks. *Green Chem.* **2017**, *19*, 5647–5652. https://doi.org/10.1039/c7gc02767b.
23. Richter, J.; Pietsch, T.; Elsner, N.; et al. Critical Investigation of Betaine Hydrochloride-Based Deep Eutectic Solvent for Ionometallurgical Metal Production. *ChemistryOpen* **2023**, *12*, e202300114. https://doi.org/10.1002/open.202300114.
24. Matsuoka, M.; Tsushima, S.; Takao, K. Fluorite-like Hydrolyzed Hexanuclear Coordination Clusters of Zr(IV) and Hf(IV) with Syn-Syn Bridging N,N,N-Trimethylglycine in Soft Crystal Structures Exhibiting Cold-Crystallization. *Inorganica Chim. Acta* **2021**, *528*, 120622. https://doi.org/10.1016/j.ica.2021.120622.
25. Yang, L.; Liu, R.; Xie, M.; et al. Construction of a MIL-101-DGA (MOF) Coupling Betaine Hydrochloride System for the Green and Efficient Separation of Zirconium and Hafnium. *ACS Appl. Mater. Interfaces* **2025**, *17*, 24369–24381. https://doi.org/10.1021/acsami.5c02082.
26. Du, C.; Ma, S.; Xie, M.; et al. Recovery of High-Value Rare Earth Elements from Waste NdFeB by the Water-Soluble Ammonium Salt [Hbet]Cl. *Sep. Purif. Technol.* **2023**, *308*, 122946. https://doi.org/10.1016/j.seppur.2022.122946.
27. Lee, J.; Fairley, M.; Goff, G.S.; et al. Quantification of Zwitterion Betaine in Betaine Bis(Trifluoromethylsulfonyl)Imide and Its Influence on Liquid–Liquid Equilibrium with Water. *Chem. Commun.* **2023**, *59*, 13599–13602. https://doi.org/10.1039/d3cc03565d.
28. Fan, F.L.; Qin, Z.; Cao, S.W.; et al. Highly Efficient and Selective Dissolution Separation of Fission Products by an Ionic Liquid [Hbet][Tf_2N]: A New Approach to Spent Nuclear Fuel Recycling. *Inorg. Chem.* **2019**, *58*, 603–609. https://doi.org/10.1021/acs.inorgchem.8b02783.
29. Yan, Q.; Liu, C.; Zhang, X.; et al. Selective Dissolution and Separation of Rare Earths Using Guanidine-Based Deep Eutectic Solvents. *ACS Sustain. Chem. Eng.* **2021**, *9*, 8507–8514. https://doi.org/10.1021/acssuschemeng.1c01616.
30. Wang, X.; Tong, Y.; Feng, W.; et al. Embedding Oxophilic Rare-Earth Single Atom in Platinum Nanoclusters for Efficient Hydrogen Electro-Oxidation. *Nat. Commun.* **2023**, *14*, 3767. https://doi.org/10.1038/s41467-023-39475-5.
31. Lan, Q.; Yang, Y.; Xie, Z.; et al. Molecular Dynamics Calculation of the Coordination Behavior of Yb(III) in Sodium Carbonate Solution. *Processes* **2023**, *11*, 2624. https://doi.org/10.3390/pr11092624.
32. Nguyen, T.T.H.; Kim, Y.H.; Lee, M.S. Selective Dissolution of Nd_2O_3 from the Mixture with Fe_2O_3 and Ga_2O_3 by Using Inorganic Acid Solutions Containing Ethylene Glycol. *Metals* **2022**, *12*, 1268. https://doi.org/10.3390/met12081268.
33. Roach, B.D.; Rogers, K.T.; Zirakparvar, N.A.; et al. The Need for Speed—Burnup Determination of Spent Nuclear Fuel. *Talanta Open* **2022**, *6*, 100152. https://doi.org/10.1016/j.talo.2022.100152.
34. Lucuta, P.G.; Verrall, R.A.; Matzke, H.; et al. Microstructural Features of SIMFUEL—Simulated High-Burnup UO_2-Based Nuclear Fuel. *J. Nucl. Mater.* **1991**, *178*, 48–60. https://doi.org/10.1016/0022-3115(91)90455-g.
35. Caprani, R.; Martin, P.; Prieur, D.; et al. Fission Products Speciation in Nuclear Fuel: Synthesis and Characterisation of Mixed Oxide (U,Pu)O_2 SIMfuel. *J. Nucl. Mater.* **2023**, *585*, 154607. https://doi.org/10.1016/j.jnucmat.2023.154607.
36. Hiezl, Z.; Hambley, D.; Lee, W.E. Preparation and Characterization of UO_2-Based AGR SIMFuel. *MRS Proc.* **2014**, *1665*, 245–251. https://doi.org/10.1557/opl.2014.651.

37. Klemettinen, A.; Adamski, Z.; Chojnacka, I.; et al. Recovery of Rare Earth Elements from the Leaching Solutions of Spent NdFeB Permanent Magnets by Selective Precipitation of Rare Earth Oxalates. *Minerals* **2023**, *13*, 846. https://doi.org/10.3390/min13070846.
38. Gong, Y.; Chen, X.; Wu, W. Application of Fourier Transform Infrared (FTIR) Spectroscopy in Sample Preparation: Material Characterization and Mechanism Investigation. *Adv. Sample Prep.* **2024**, *11*, 100122. https://doi.org/10.1016/j.sampre.2024.100122.
39. Subiarto, B.G.; Clyde, D.A.; Yiang, W.J.; et al. Facile Valorization of Hazardous Lithium-Ion Battery Waste: Betaine Hydrochloride-Based Deep Eutectic Solvent as a Green Platform for Heavy Metal Extraction. *J. Environ. Chem. Eng.* **2025**, *13*, 119377. https://doi.org/10.1016/j.jece.2025.119377.
40. Wang, B.; Duan, Y.; Gong, S.; et al. Green Deep Eutectic Solvents for Lithium-Ion Battery Cathode Black Powder Impurity Removal and Precious Metal Recovery. *Energy Fuels* **2025**, *39*, 9601–9610. https://doi.org/10.1021/acs.energyfuels.5c00677.
41. Luo, Y.; Ou, L.; Yin, C. Extraction of Precious Metals from Used Lithium-Ion Batteries by a Natural Deep Eutectic Solvent with Synergistic Effects. *Waste Manag.* **2023**, *164*, 1–8. https://doi.org/10.1016/j.wasman.2023.03.031.
42. Tian, G.; Martin, L.R.; Rao, L. Complexation of Lactate with Neodymium(III) and Europium(III) at Variable Temperatures: Studies by Potentiometry, Microcalorimetry, Optical Absorption, and Luminescence Spectroscopy. *Inorg. Chem.* **2010**, *49*, 10598–10605. https://doi.org/10.1021/ic101592h.
43. Ding, A.; Liu, C.; Zhang, X.; et al. $ZnCl_2$: A Green Brønsted Acid for Selectively Recovering Rare Earth Elements from Spent NdFeB Permanent Magnets. *Environ. Sci. Technol.* **2022**, *56*, 4404–4412. https://doi.org/10.1021/acs.est.1c08260.
44. Liu, C.; Yu, J.; Hu, J.; et al. Ultra-Low Viscosity Betaine Hydrochloride-Formic Acid Deep Eutectic Solvent for Leaching Critical Metals from Spent NCM Lithium-Ion Batteries. *J. Environ. Chem. Eng.* **2024**, *12*, 112586. https://doi.org/10.1016/j.jece.2024.112586.
45. Gholami, S.; Pérez-Page, M.; D'Agostino, C.; et al. (Deep) Eutectic Solvents for the Separation of Platinum Group Metals and Rare Earth Elements: Characteristics, Extraction Mechanisms and State of the Art. *Chem. Eng. J.* **2025**, *505*, 159497. https://doi.org/10.1016/j.cej.2025.159497.
46. Di Gioacchino, M.; Bruni, F.; Ricci, M.A. Aqueous Solution of Betaine: Hydration and Aggregation. *J. Mol. Liq.* **2020**, *318*, 114253. https://doi.org/10.1016/j.molliq.2020.114253.
47. Mayanovic, R.A.; Anderson, A.J.; Bassett, W.A.; et al. The Structure and Stability of Aqueous Rare-Earth Elements in Hydrothermal Fluids: New Results on Neodymium(III) Aqua and Chloroaqua Complexes in Aqueous Solutions to 500 °C and 520 MPa. *Chem. Geol.* **2009**, *259*, 30–38. https://doi.org/10.1016/j.chemgeo.2008.08.011.
48. Kremer, C.; Torres, J.; Domínguez, S.; et al. Structure and Thermodynamic Stability of Lanthanide Complexes with Amino Acids and Peptides. *Coord. Chem. Rev.* **2005**, *249*, 567–590. https://doi.org/10.1016/j.ccr.2004.07.004.
49. Kutus, B.; Varga, N.; Peintler, G.; et al. Formation of Mono- and Binuclear Neodymium(III)–Gluconate Complexes in Aqueous Solutions in the pH Range of 2–8. *Dalton Trans.* **2017**, *46*, 6049–6058. https://doi.org/10.1039/c7dt00909g.
50. Wang, Z.; Lu, J.B.; Dong, X.; et al. Ultra-Efficient Americium/Lanthanide Separation through Oxidation State Control. *J. Am. Chem. Soc.* **2022**, *144*, 6383–6389. https://doi.org/10.1021/jacs.2c00594.
51. Veliscek-Carolan, J. Separation of Actinides from Spent Nuclear Fuel: A Review. *J. Hazard. Mater.* **2016**, *318*, 266–281. https://doi.org/10.1016/j.jhazmat.2016.07.027.
52. Zhang, H.; Li, A.; Li, K.; et al. Ultrafiltration Separation of Am(VI)-Polyoxometalate from Lanthanides. *Nature* **2023**, *616*, 482–487. https://doi.org/10.1038/s41586-023-05840-z.
53. van Til, S.; Hania, P.R.; Fedorov, A.V.; et al. Irradiation Performance and First Examinations of Americium Bearing Blanket Fuel from the MARINE Irradiation Experiment. *J. Nucl. Mater.* **2023**, *587*, 154699. https://doi.org/10.1016/j.jnucmat.2023.154699.
54. Herrmann, S.D.; Li, S.; Westphal, B.R. Separation and Recovery of Uranium and Group Actinide Products from Irradiated Fast Reactor MOX Fuel via Electrolytic Reduction and Electrorefining. *Sep. Sci. Technol.* **2012**, *47*, 2044–2059. https://doi.org/10.1080/01496395.2012.697511.
55. Einkauf, J.D.; Burns, J.D. Recovery of Oxidized Actinides, Np(VI), Pu(VI), and Am(VI), from Cocrystallized Uranyl Nitrate Hexahydrate: A Single Technology Approach to Used Nuclear Fuel Recycling. *Ind. Eng. Chem. Res.* **2020**, *59*, 4756–4761. https://doi.org/10.1021/acs.iecr.0c00381.
56. Fan, F.L.; Chen, D.S.; Huang, Q.G.; et al. Radiation Effect on Ionic Liquid [Hbet][Tf_2N] for Nd_2O_3 Separation from Simulated Spent Nuclear Fuels. *J. Radioanal. Nucl. Chem.* **2020**, *326*, 497–502. https://doi.org/10.1007/s10967-020-07306-2.